Hydrothermal processes, fluid systems, metasomatism

Korzhisky M.A., Zhdanov N.N., Tkachenko S.I., and Botcharnikov R.E. Anomalous hydrogen m volcanic gases of Kudriavy Volcano, Iturup Island, South Kuriles (Direct Measurements)

key words: [*volcanic gas direct measurements monitoring hydrogen*]

We pioneered continuous direct measurements of high temperature (up to 900°C) volcanic gas conditions under automatic operation at Kudriavy volcano (South Kuriles) from September 20 to October 11, 1998. A combined sensor apparatus designed and built in the Institute of Experimental Mineralogy RAS was used. The arrangement and main operation principles of sensors, pressure transducers and overall system arc described in [1]. Temperature of fumarole gases, gas pressure in volcanic channel, and partial hydrogen pressure in high temperature gas jet were measured during mentioned period at one of the high temperature fumarole fields. Ambient temperature, atmospheric pressure, and precipitation were measured as well. The obtained results are shown in Fig. 1.

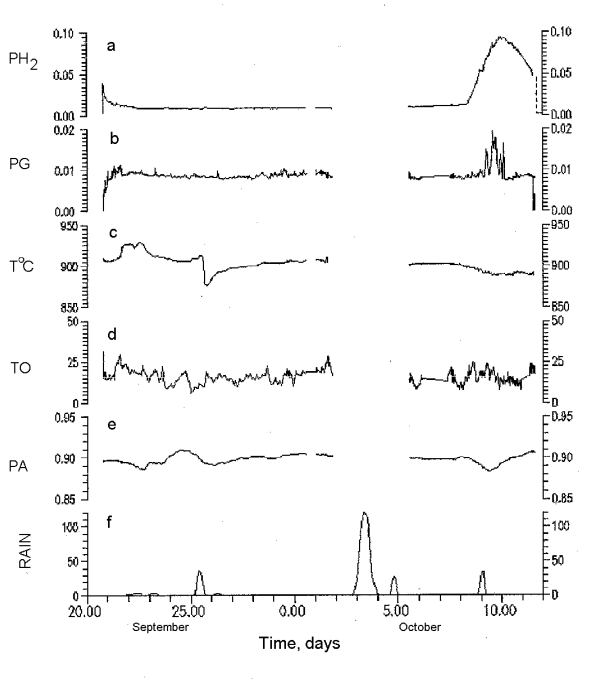

Fig.1. Results of high temperature volcanic gas condition measurements at Kudriavy volcano (pressure in bars, temperature in °C). a) partial hydrogen pressure in volcanic gas (dashed line stands for the measurements completed in laboratory over a month); b) excess gas pressure in volcanic channel; c) temperature of the "940" fumarole; d) ambient temperature; e) atmospheric pressure; f) precipitation (mm H_2O).

The main and unexpected result of the performed measurements is a record of very high hydrogen discharge at Kudriavy volcano. The hydrogen concentration $X_{H2}=P_{H2}/P_{total}$ was about 1 mole% during a long time but since October 8 till October 10 it had spontaneously increased up to 10 mole%. The total duration of elevated hydrogen discharge was about 4-4.5 days. At the same time there was observed a spontaneous increase of gas pressure in volcanic channel from 80 mm H_2O (in a quiet period) up to 180 mm H_2O. The temperature of volcanic gases had no significant changes. Its local decrease in September 25 was caused by meteoric water precipitation. The data plotted in Fig. 1 indicate no correlation between the high hydrogen discharge and ambient conditions (temperature, atmospheric pressure and precipitation). Such a great concentration of hydrogen in volcanic gases is anomalous. Usually, hydrogen content in high temperature volcanic gases, sampled by conventional methods, is not above 1-2 mole%. The observed hydrogen concentrations at Kudriavy volcano can not be explained by equilibrium processes between gas and silicate melt. The H_2; content in volcanic gases in equilibrium with quartz -magnetite - fayalite mineral association at the magmatic temperature and and P = 1 bar is about 1 mole%. The performed measurements demonstrate that outgassing conditions at Kudriavy volcano have discrete-pulsating character. It is suggested that endogenous processes, occurring in subsurface magma chamber and governed by local ascent of fresh magmatic melt, may be responsible for the high discharge of hydrogen. These processes might be caused by seismic events fixed at seismic station in Kurilsk (Iturup Island) (of magnitude 2 on the Richter scale in the radius 100-110 km) in October 6,7, and 8.

Reference:

1. Korzhinsliy, M.A., N.N. Zhdanov, S.I. Tkachenko, and R.E. Botchamikov (1999) New equipment for Ihe measurements of high temperature volcanic gas conditions. // Experiment in Geosciences, V.8, Nl. p.71

#Lebedev E.B., Ryzhenko B.N., Dorfman A.M., Zharikov A.V., Sokolova N.T.,

The work has been sponsored by the RFBR (grants N 98-05-64768 and N 99-05-65698)

Shmonov V.M. Experimental study of influence of water fluid composition on the elastic properties of sandstone at high pressures and temperatures, and computer modeling of the water-rock interaction.

key words [*experiment elastic wave velocities fluids acido-basic properties rock microstructure porosity permeability high pressures temperatures*]

The obtained experimental data have shown that brines with various acid-alkali properties affect noticeably the velocity of elastic waves in sandstone in the temperature range 100-850°C under a pressure 300 MPa .

Extreme points on temperature dependencies of the velocities of elastic waves in sandstone under a fluid pressure can be attributed to rock transformation due to a number of concurrent chemical reactions and processes: metasomatic reactions, rock quartzization processes, phase transformations.

The character of elastic waves propagation in a rock is related to a change in its microstructure, a change in porosity and permeability. An increase of microcracking and volume of a pore space of sandstone produces a decrease of the elastic waves velocity. Closing of microcracks and formation of a more rigid rock structure due to the appearance of new hydrothermal layered minerals leads, on the contrary, to an increase of the elastic waves velocity.

There is a correlation of the dependencies of the elastic waves velocity and sandstone porosity at a change in the acido-alkali properties of fluids (NaOH, Na_2CO_3, and H_2O) in the temperature range of 200-400°C and pressure 300 MPa, fig.1

The obtained results have also shown a noticeable influence of the fluid composition in the series: NaOH - Na_2CO_3 -Na_2HCO_3, and H_2CO_3 on the elastic properties of sandstone. This is likely due to the proceeding mineral reactions producing alterations in the rock microstructure. Consequently, fluids at a change in their chemical composition with a gradual regular alteration of the acido-alkali properties or a change in the pH of the solution due to the water-rock interaction can affect the elastic properties of sandstone.

The experimental data suggest that an increase in the elastic waves velocity of sandstone in the temperature range of 140-400°C in the presence of alkali and carbonate fluids can be attributed to rock transformations produced by reactions of partial dehydration of kaolinite and the formation of mica.

The above proposed interpretation of a change in the elastic waves velocities in sandstone at elevated temperatures is confirmed by the data on a synchronous alteration of porosity and permeability, the porosity values for a Na_2CO_3 fluid being intermedia between those of NaOH and H_2O fluids at T=100-300°C. In order to estimate alterations in the fluid phase and the mineral rock composition resultant from the experiments, we have performed a physicochemical computer modeling of an equilibrium composition of the system in question: sandstone/water fluids. The experimental data enable us to prospectively estimate the influence of the fluid components, of pH of the solution, and, mass rock/water ratio on the elastic properties of rock, fig.2. At a particular mass rock/water ratio equal, e.g., to 1 at P=300MPa and T=300°C with a change in the fluid pH from 1 to 5-6 the elastic waves velocity will be roughly constant, close to 3.3-3.2 km/s. As pH=6 grows to 9, the elastic waves velocity will grow to 3.7-3.8 km/s.

The experimental model data can be used for a geochemical interpretation of anomalies of seismic velocities documented in the middle part of the continental crust.

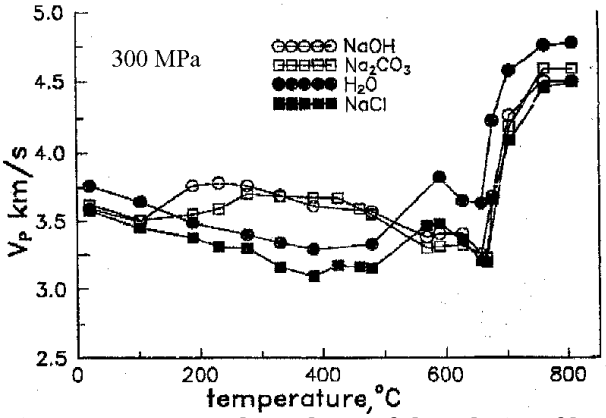

Fig.1. Temperature dependence of the velocity of longitudinal elastic waves (V_p) in sandstone under of pressure of brines (NaOH, Na_2CO_3, NaCl, H_2O), 300MPa.

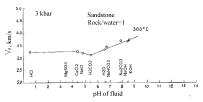

Fig.2. Supposed change in V_p with a fluid pH growth from 1 to 9. Rock/water ratio=1.

Reference:

1. Lebedev E.B., Ryzhenko B.N., Dorfman A.M. et al (1996) Influence of fluids on the elastic properties of sandstone at high pressure and temperature. // Geophysical Research Letters, V.23, N. 22, pp.3115-3118.

#Pal'yanova G.A., Shironosova G.P., Kolonin G.R.,Tsimbalist V.G. Monohydrosulfide complex $AuHS^o$: thermodynamic analysis of the available and new experimental data.

key words: [*gold solubility acid sulfide solutions HKF parameters experimental checking minerals buffers gold-silver alloys*]

A largest number of experimentalists [1-5] who deal with acid sulfide solutions assume that at moderate concentrations of chloride ion in them the prevailing from of occurrence is neutral monohydrosulfide complex $AuHS^o$. Even so, the corresponding thermodynamic values and HKF parameters are nevertheless tacking for this complex in recent works too [6,7] which imposes limitations on the development of present-day theoretical models of formations of gold-bearing deposits.

The work was sponsored by the RFBR (Project N 97-05-65252)

To solve this problem we processed the values of free Gibbs energies of the $AuHS^o$ complex in the temperature range of 25-450°C (UT-HEL program of the Hch computer considering the available experimental works [2-5,8]. Thus derived preliminary HKF parameters were refined by the HELGESON program (H.H.Akinfiev)). An important moment of our computations is the assumption that the Born coefficient ω for $AuHS^o$ is taken to be -0.038 by analogy with more reliably studied neutral complexes $AgOH^o$ and $AgCl^o$. Such assumption seems valid since all these forms can be described by the same type of exchange reactions $M_1L_1 + M_2L_2 = M_1L_2 + M_2L_1$, whose enthalpic and other thermodynamic effects ought to be quite close to zero. The derived HKF parameters of $AuHS^o$ are listed in table 1 together with standard thermodynamic characteristics at 25°C, 1 bar.

Table 1. Standard thermodynamic characteristics and HKF parameters of $AuHs^o$ taken in this work.

Δ_fG^{o298} cal/mol	6117
S^o_{298} cal/mol·K	43.23
$C_{P,298}$ cal/mol·K	-15.76
V_{298} cm^3/mol	19.28
$a_1 \cdot 10$ cal/mol·bar	4.3888
$a_2 \cdot 10^{-2}$ cal/mol	2.935
a_3·cal·K/mol·bar	4.5961
$a_4 \cdot 10^{-4}$ cal·K/mol	-2.9003
$c_1 \cdot 10^{-4}$ cal·K/mol	-3.4159
$c_2 \cdot 10^{-4}$ cal·K/mol	-6.2449
$\omega \cdot 10^{-5}$ cal/mol	-0.038

In order to additionally check the derived values and to estimate the possibilities of their use for solving particular problems of thermodynamic modeling, we performed the runs (T=350°C, P=0.5 kbar) on solubility of gold-silver alloys of various compositions in chloride-sulfide solutions in the presence of mineral buffers (quartz-muscovite-K-feldspar-pyrrhotite-magnetite (Py-Po-Mt)). Gold-silver alloys were used thereat not only as starting solvents but also as intrinsic universal indicators of sulfide sulfur and redox conditions [9]. An analytic determination of Au and Ag in the solution was performed by a method of atomic absorption with preliminarily concentrating the metals by organic extragents. The starting composition of gold-silver alloys in the runs ranged from 0.2 to 0.7 mole fraction of silver (N_{Ag}). Its change after the runs was controlled by a microprobe analysis. The 1.0 m KCl+0.1 m HCl solution was the starting one. The run duration was 30 days.

Table 2. Results of comparison between the experimental and calculated data on solubility of gold-silver alloys of different composition in acid chloride solutions (for conditions see in the text)

Composition of solution and sold phases		Starting composition of the alloy (N_{Ag})		
		0.2	0.3	0.7
m_{H2S}	Exper.	0.012	0.0142	0.0140
	Calcul (Py-Po)	0.00913	0.00913	0.00913
m_{H2}	Exper. (estim. in m_{Ag})	$(2.8\pm0.35)\cdot10^{-5}$	$(3.01\pm0.13)\cdot10^{-5}$	-
	Calcul. (Py-Po-Mt)	$4.43\cdot10^{-4}$	$4.43\cdot10^{-4}$	$4.43\cdot10^{-4}$
m_{Au}	Exper.	$(3.75\pm0.14)\cdot10^{-6}$	$(2.90\pm0.75)\cdot10^{-6}$	$(1.86\pm0.20)\cdot10^{-6}$
	Calcul.	$1.4\cdot10^{-6}$	$1.2\cdot10^{-6}$	$8.7\cdot10^{-7}$
m_{Ag}	Exper	$(5.61\pm0.69)\cdot10^{-5}$	$(5.99\pm0.26)\cdot10^{-5}$	$(5.31\pm2.23)\cdot10^{-4}$
Final compos. of solid phases		$NAg_{0.17}$	$NAg_{0.21}$	$NAg_{0.40+0.20}+Ag_2S$
Results of run processing	log $K_{dissolution}$	-5.71±0.04	-5.86±0.12	-
	G $AuHS^o$, kcal/mol	-6.87±0.10	-6.43±0.34	-
	log$K_{dissotoation}$	-13.35±0.04	-13.20±0.12	

The Au-Ag-Na-Cl-S-H_2O system's database containing the required information for 39 dissolved particles and 14 solid phases was developed for the thermodynamic calculations modeling the runs. Along with the SUPCR T92[10] we used the data of [6,7] for chloride and sulfide complexes of silver and gold, for hydroxocomplexes of silver, and the calculated by us thermodynamic characteristics of $AuHS^o$ and $AgHS^o$ particles (defined for the latters by the same technique as for $AuHS^o$ complex). which had been lacking in those works. The thermodynamic data for HCl^o were borrowed from [11]. Finally, G_T for gold-silver alloys were calculated using the equation of [12] with allowance for the activity of Au and Ag at a step of 0.1 molar fraction. Note, that the calculations were performed at a pressure 1 kbar under the open-system conditions at preset O_2 and S_2 fugacities corresponding to a Py-Po-Mt buffer, in accordance with [13].

The compositions of the solutions and sold phases are listed in table 2 together with the results of the thermodynamic calculations. The runs and the calculations are in good conformity in gold concentration, redox potential, sulfide sulfur. Under the assumption that in acid solutions the dissolution of gold from an alloy-proceeds by the reaction $Au_{alloy} + H_2S^o_{aq} = AuHS^o + 0.5H_{2aq}^o$ and can be described by the equation $\log K = \log m_{Au} + 0.5\log m_{H2} - \log m_{H2S} = -\log a_{Au(alloy)}$, its experimental constants is logK=5.74±0.22. With this value we obtained the G value for $AuHS^o$ at T=350°C and logK for this complex dissociation to be -13.35±0.12.

In our opinion these values are reliable not only because of proximity of the experimental and calculated data but also in view of their position practically coincident with the pK values of dissociation under saturated vapour pressure and 0.5 kbar form [4] (see the figure). At the

same time they are by approximately 1 order higher than the results of [5] and [8] (after our recalculation of the latters to a $AuHs^o$ particle instead of the $HAu(HS)_2^o$ complex).

References:

1. Seward T.M. (1973) //Geochim. Cosmochim. Acta. . V. 37, pp. 379-399.
2. Renders P.J., Seward T.M. (1989) // Geochim. Cosmochim. Acta. . V.52. pp. 245-253.
3. Bening J.G., Seward T.M. (1996) //Geochim. Cosmochim. Acta. V.60. pp. 1849-1872.
4. Gibert F., Pascal M.-L.. Pichavant M. (1993) // Proceed, of the 4th ISHR. Nancy. pp. 65-68.
5. Baranova N.N., Zotov A.V. (1998) //Mineralogical magazine. V.62a. p. 116-117.
6. Sverjensky D.A., Shock E.L.. Helgeson H.C. (1997) //Geochim. Cosmochim. Acta. V.61, p.1359-1412.
7. Shock E.L., Sassani D.C., Willis M. et.al. (1997) // Geochim. Cosmochim. Acta. V.61, pp.907-950.
8. Hayashi K., Ohmoto H. (1991) // Geochim. Cosmochim. Acta. . V. 55. pp. 2111-2126.
9. Gammons @ Williams-Jones (1995) // Geochim. Cosmochim. Acta, , V. 59, pp.3453-3468.
10. Johnson J., Oelkers E., Helgeson H. (1992) //SUPCRT-92 //Computers Geosci. . V. 18. pp. 899-947.
11. Sverjensky D.A., Hemley J.J., D'Angelo. (1991) //Geochim. Cosmochim. Acta. . V.55,p.989-1004.
12. White J.I., Orr R.L., Hultgren R. (1957) //Acta Metallurgica. V.5, , p.747-760.
13. Hishima N. (1989) // Geochim. Cosmochim. Acta. . V.53, p.2143-2155.

#Kiseleva I.A. Stilbite - heulandite equilibrium as derived from thermochemical data.

key words [*thermochemistry phase equilibria heulandite stilbite zeolites*]

Equilibrium of widely occurring in nature calcium silicon-rich zeolites - stilbite and heulandite, given by the reaction: $CaAl_2Si_6O_{18}\cdot 7H_2O$ (stilbite) = $CaAl_2Si_7O_{18}\cdot 6H_2O$ (heulandite) + H_2O is important for considering low temperature formations of zeolite facies.

An experimental approach to a study of zeolite facies minerals equilibria encounters considerable kinetic difficulties at reaching equilibria. In this work we used a thermodynamic approach to study equilibria based on an experimental calorimetric determination of thermochemic characteristics directly for the reaction itself and for the minerals involved in it. Methods of high temperature dissolution calorimetry were used to study natural stilbite and heulandite. The enthalpy of the reaction was defined from the obtained thermochemic data.

The free Gibbs energy and the P-T equilibrium conditions were calculated using the entropy data from equilibria and calorimetry runs.

A stilbite - heulandite equilibrium has not yet been studied experimentally. The position of this equilibrium in the P-T co-ordinates for the calcium part of the system was contemplated in the work by Cho et al, 1987, who studied the upper temperature limit of heulandite stability, its equilibrium with lanmontite and quartz. The authors conjectured the position of the triple point to be approx. at 600 bar and 140°C.

The stilbite and heulandite studied (Nydym, East. Siberia) are compositionally close to calcium varieties of the theoretical composition. The crystallochemical formulas recalculated to 18 oxygen atoms are: stilbite - $Ca_{1.01}Na_{0.12}(Al_{2.12}Si_{6.88}O_{18})\cdot 7.27H_2O$, heulandite - $Ca_{0.86}Na_{0.37}K_{0.06}(Al_{2.14}Si_{6.86}O_{18})\cdot 6.10H_2O$.

The enthalpies of solution of minerals studied were determined using a Tian-Calvet high-temperature heat-flux microcalorimeter. The samples were dropped from room temperature into molten 2 $PbO\cdot B_20_3$ at 975 K. The heat of drop solution was a sum of the heat of solution in the melt plus the heat content. All experiments were performed under a dry-air atmosphere flowing through the calorimeter.

The calorimeter measurements yielded the value of $[(H^o_{975}-H^o_{298.15}) + \Delta H^o_{sol\cdot 975}]$ for natural stilbite to be 1092.5±9(8) and for heulandite 1001.6±4.3(8) kJ/mol. Since we studied natural samples having deviations from stoichiometry, we corrected the experimental data to the ideal stoichiometry of calcium varieties. ΔH^o of the stilbite-heulandite reaction, calculated from the experimental data, was equal to 19.8+8.8 kJ/mol. The entropy of the reaction was calculated using the standard entropy value of calcium heulandite derived from its experimentally studied equilibrium with laumontite and quartz (Cho et al) - 783.7 J/mol·K. The standard entropy value of calcium stilbite (795.1 J/mol·K) was recalculated from the experimental calorimetric data (Howell at al, 1990) by correction to ideal stoichiometry.

The values of the thermodynamic parameters of the reaction, calculated for 298.15K are: $\Delta S^o r$ =58.6 J/mol·K, $\Delta V^o s$=1.6 J/mol·bar, $\Delta G^o r$ = 2.4 kJ/mol.

The calculated curve of a stilbite-heulandite equilibrium (ΔCp of the reaction is 0, and the solid phases volume is constant) under the condition P_{H2O}=Ps goes at temperatures 120-135°C for pressures 1-5 bar which agrees well with the equilibrium line contemplated by Cho et al., 1987, and with the invariant point at 600 bar and 140°C, fig.1. The calculation of equilibria of stilbite and heulandite containing alkalies, especially sodium, shows an increase in the equilibrium temperature by approx. 100-150°C. The compositional variations of natural stilbite and heulandite are thus noticeably reflected in the temperatures of their equilibrium.

The work was sponsored by the RFBR (Grant N 98-05-64219)

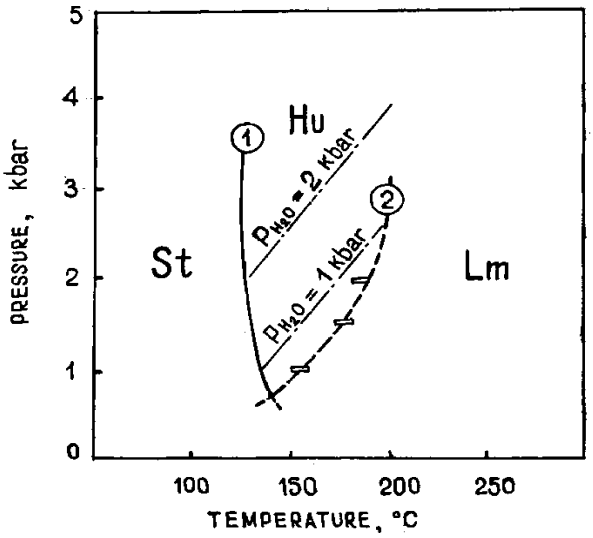

Fig.1 Phase relations among stilbite (St),heulandite (Hu) and laumontlte (Lm). 1-reaction: stilbite = heulandite + H_2O is calculated from thermochemical data in this study; 2 - reaction: heulandite = laumontite + 3 quartz + 2 H_2O is studied by (Choet. al., 1987)

Micuk B.M. The change of solubility of silica amorphous modifications in the process of hydrothermal treatment at 250°C

key words:[*silicage, opal solubility*]

To elucidate a silica material transport mechanism under the conditions of Earth's crust, we performed a study of solubility behavior of silicagel and opal-like amorphous silica forms in a pure water and in 0.1N HCl solution in a wide temperature range up to 250°C. It was taken into account that silicagel pore structure undergoes significant changes during the process of hydrothermal treatment. The dimensions of pores and primary globular particles increase and, as a consequence, specific surface drastically reduces. The 'aging' and densification of silica material proceed as a formation of opal-like structures with the wide variations of globular particle sizes.

In this study we attempted to elucidate the influence of those structural changes on the solubility and dissolution kinetics of amorphous silica. A comparable study of the solubility of silica amorphous forms in pure water and diluted HCl solution was encouraged by the fact that the presence of acid inhibits the process of silica material transport and its redistribution in globular structure. This process is particularly intensive in pure hydrothermal solutions.

It was revealed that silicagel solubility in pure water and 0.1N HCl solution almost linearly enhanced with temperature up to 250°C. However, the equilibrium solubility at 80 and 120°C was not achieved in pure water as well as in HCl solution despite the duration of experiments was 27 and 23 days, respectively. At 150 and 200°C, the equilibrium values in pure water were obtained only in the runs lasted by 20-30 days longer than experiments in 0.1N HCl solution. However, the samples, subjected to a long-term hydrothermal pretreatment, were equilibrated with the solution much more rapidly.

An increase of silicagel dissolution rate in the acid environment is a result of the aging process slowing down and retention of large specific surface of the samples. At the same time, the intensive redeposition of silica material occurs in pure water facilitating the size enhancement of primary silicagel globular particles and consequently a decrease in specific surface of the samples. Therefore, the dynamic equilibrium of solubility in water is not attained until the mentioned above processes are completed and dissolved silicic acid is not consumed in these processes.

In fact, the specific surface of the samples in pure water decreased from 640 to 120 m^2/g while in the acid solution just to 400 m^2/g. The greater increase of particle sizes in pure water led to more profound decrease in solubility of the corresponding opal sample to 27 mg/l (after 123-day dissolution process at room temperature) and to 41 mg/l (after 7-year experiment) in comparison with solubility of starting highly active silicagel. Its solubility value was around 110 mg/l. In the latter case, the extreme solubility was achieved in the first 50-70 hours. On the other hand, the opal sample obtained in the acid environment displayed high solubility: 75 and 102 mg/l corresponding to runs with the duration of 123 days and 7 years.

These data testify to a change in physical chemical properties of the silica surface with increasing the globule size which leads to reducing the free surface energy of the particles. As this takes place, a share of siloxan bounds ≡Si–O–Si≡ in the inner structure of the gel particles increases. It leads to an increase in the strength of surface silanol bounds ≡Si–OH. Moreover, the significant structural ordering of silicon-oxygen tetrahedrons occurs due to reducing the curvature of the globule outer surface. As a consequence, it favors the enhancement of inertness of the silicon-oxygen bounds and decrease of opal-like silica solubility. It must be noted that both opal samples are amorphous and do not have a long-range structural order.

Thus, in the process of hydrothermal treatment of silicagel the branched net of silicon-oxygen bounds forms, the share of siloxane bounds increases whereas the portion of silanol groups reduces. This facilitates the increase in degree of 'homogeneity' of the silica material and thus the decrease in its solubility.

Koval V.B., Samsonov V.A., and Starikov V.G. Transformations of feldspars at alkali metasomatism (from experimental data)

key words: [*potash feldspar microperthite metasomatism albite microcline orthoclase*]

Natural alkali feldspar from Volynsk pegmatites was used as a starting material to perform the experimental series (fraction powder 0.5+0.25 mm). By optical methods, it was determined that this mineral contains two crystalline phases: (1) microcline with n_p = 1.514, n_g = 1.521; (2) albite with n_p = 1.520, n_g = 1.524. The presence of three mineral phases (albite, microcline and orthoclase) was revealed by x-ray aanalysis of powder samples. The last phase was not clearly distinctive due to its paucity in the sample.

The sample charge was taken so that the ratio of solution mass to solid phase mass was constant at different temperature conditions. During experimental procedure, it was found that ratio equal to 6 is most reasonable for the given duration (96 hours). Interaction between microperthite and alkali-carbonaceous solutions proceeded in autoclaves (volume 20 cm^3) and exoclaves (volume 120 cm^3) at temperatures from 200 to 500°C and pressure 30 MPa. The accuracy of temperature measurements was ±5°C. The degree of autoclave filling was selected so that pressure was about 30 MPa taking into account data from [3]. The coefficients of filling are presented in table only because of the lack of information for concentrated solutions. In cases when experiments were performed in exoclaves at temperatures 300 and 500°C, pressure was produced by hydraulic pump like HRP-1 type and maintained at constant level (30±2) MPa with the help of electrocontact pressure gauge EKM-1. The optimal time of microperthite exposure in auto- and exoclaves (96 h) was chosen based on our experiments for studying equilibrium between solution and solid phase at different P,T-conditions. The identical new phases were observed in experiments in both autoclaves and exoclaves. 40% solution of K_2CO_3 was used as alkali-carbonaceous solution.

Table. The dependence of pressure vs the temperature, filling coefficient and composition of solution. The first four runs were conducted in autoclaves, the others - in exoclaves.

Temperature, °C	Pressure, MPa	Filling coefficient	Volume of solution, cm^3	Sample weight, g
200	-	0.92	18.4	3.07
300	-	0.84	16.8	2.80
400	-	0.55	11.0	1.83
500	-	0.4	8.0	1.33
300	30	-	-	20.0
500	30	-	-	20.0

The newly formed mineral phases were determined by optical (in immersion liquids) and x-ray methods. The conditions of experiments and their results are presented in table.

The experiments showed that at interaction of 40% K_2CO_3 solution with microperthite the formation of new crystalline phases was observed all over the temperature range. The higher temperature, the more intensively this process proceeded. The exception was the runs performed at temperature 200°C. After those experiments, the individual grains of newly formed mineral compounds, growing on albite, were identified in the solid phase. The indexes of reflection for new phase were as follows: n_p = 1.560; n_g = 1.566. The optical methods testified about kaolinite formation though possibility of appearance for some mineral of zeolite group was not excluded [4]. Chemical analysis of solutions after runs at that temperature revealed significant concentrations of SiO_2 and Na_2O.

At temperature 300°C, the formation of new crystalline phase was identified more clearly. It grew on initial albite grains as a 'fringe' of plate-like shape or partly substituted the grain itself. In the starting albite, the gas-liquid inclusions were observed, whereas the new phase was pure with the indexes of reflection as n_p = 1.518 and n_g = 1.525 (orthoclase). The concentration of SiO_2 and Na_2O in solution after runs was higher than at temperature 200°C.

Temperature increase up to 400°C led to drastic enhancement in quantity of new phase with the same indexes of reflection as in the previous run series. The newly formed mineral phase grew on albite, covering all grain by the plates of hexagonal or prismatic acicular shape (orthoclase). The concentration of SiO_2 and Na_2O in solution after runs increased. Almost complete substitution of albite for potash feldspar was observed as temperature increased up to 500°C. The concentration of SiO_2 and Na_2O in solution after experiments was above tenths of grams per liter.

It is known [1, 2, 6] that a compound like $KalSi_3O_8$ can exist in three modifications: high-temperature (sanidine), medium-temperature (orthoclase) and low-temperature (microcline). The optical data of our investigations could not clearly testify to the formation of one or another type of potash feldspars at given temperature conditions. However, in all run series, starting microcline was almost not altered. The optical method of microcline investigations revealed its absolute identity with the initial phase. Thus, the formation of a new phase may be related only to albite substitution for potash feldspar.

To ascertain the more precise diagnosis, the x-ray investigations were performed. The x-ray analysis of microperthites in the x-ray patterns of starting mineral powder (sample 1) and also after runs at temperatures 300°C (sample 2) and 400°C (sample 3) showed their significant differences due to substitution of initial mineral. The x-ray patterns for powder samples were obtained on diffractometer DRON-2.0. CuK_α-radiation was used with Ni-filter at a voltage of 30 kV and current of 30 mA; scale 400 imp/s. Germanium (a=0.56576 nm) was used as an inner standard with reflections 220 and 311.

The results of x-ray phase analysis of reaction products showed, that they consist of orthoclase, microcline, sometimes albite. To evaluate their ordering, the x-ray analysis was conducted in the following 2Θ intervals: 20-23°; 29-31.5°, 41.2-43°; 45-46°; 50.3-51.3°; 53.5-54°. A diagnosis of phase composition and ordering of feldspars was carried out on the basis of reflections $\bar{2}01$, III, 131, $1\bar{3}1$, 060, and $\bar{2}04$.

$\bar{2}01$ reflexes testify to the presence of potash feldspar and albite in sample 1 but reflections III, 131 and $1\bar{3}1$ are responsible for the presence of monoclinic and triclinic phases of potash feldspar. Reflections 060 and $\bar{2}04$ of orthoclase were not detected due to paucity of this mineral in the sample. A ratio of amplitudes of albite and potash feldspar $\bar{2}01$ reflections corresponds to almost equal quantity of these phases in the sample [5].

The microcline and albite ordering (samples 1-3) was evaluated by a technique described in [2]. Due to superposition of 131 reflections for those minerals, the atomic fraction of aluminum t_1 in aluminum-silicon-oxygen tetrahedrons T_1o and T_1m can be only determined: $t^{Mic}_1 = 0.93$; $t^{Ab}_1 = 0.99$. The chemical composition of microcline and albite can be identified from the double angle of reflection $\bar{2}01$ because those minerals were not anomalous. Microcline chemical composition was equal to 97% Or but albite around 0% Or. Hereinafter, Or is a content of orthoclase molecule in alkali feldspar, determined with an accuracy of 4%.

The x-ray pattern of sample 2 powder was characterized by a marked decrease in albite $\bar{2}01$ and 060 reflexes while reflections 131, 041 and $\bar{2}04$ at given analytical operations were not registered. Moreover, 131 the orthoclase reflection significantly increased and 060 and $\bar{2}04$ reflections appeared near the similar reflections of microcline. The type of x-ray pattern allows to conclude that albite quantity in the sample is negligible. The determination of potash feldspar ordering was not possible due to superposition of 060 and $\bar{2}04$ reflexes of orthoclase and microcline. In the sample 2, composition of potash feldspar phase was equal 98% Or but albite phase was around 0% Or.

The $\bar{2}01$ reflection of sample 3 x-ray pattern testified to even lower albite content. The more clear separation of III, 060 and $\bar{2}04$ reflections of microcline and orthoclase than in sample 2 was observed. Here, the composition of potash feldspar phase was also equal 98% Or. It was not possible to determine the albite composition due to superposition of intensive microcline III reflection on weak $\bar{2}01$ reflection of albite.

In the whole, the x-ray patterns of three samples are indicative of the preferred enhancement of orthoclase phase with temperature at a given salt composition of the solution. The evidence is $I_{111}{}^{Mic}/I_{111}{}^{Or}$ ratio, which is equal to 1.42 in sample 1, 1.35 in sample 2, and 1.22 in sample 3. The chemical composition of potash feldspar and albite phases did not change.

The results of performed investigations testify that interaction between 40% K_2CO_3 solution and microperthite, where potash feldspar constituent is presented by microcline and orthoclase, leads to almost full substitution of albite for orthoclase at temperature 500°C and pressure 30 MPa. The results of chemical analyses of solutions after runs suggest that concentrated potash carbonate solutions are able to form the sodium-potassium carbonaceous solutions saturated with silicon during ion exchange reactions. The concentration of mentioned above elements in solutions is up to ten grams per liter. Aluminum in this process is inert. This is supported by the reaction of albite substitution in microperthite for potash feldspar.

The described substitution reactions allow to significantly refine the formation scheme of alkali metasomatites in Precambrian shields, outline the restoration criterions of temperature regime from peculiarities of mineral composition, and confirm the earlier conclusion about alkali-carbonaceous composition of solutions.

References:

1. Bregg W., Claringbull G. Crystal structure of minerals. M.: Mir, 1967, p. 390 (in Russian).
2. Kamencev I.E. and Smetannikova O.G. The determination of Al-Si ordering and composition of feldspars by powder method. Zap. Vsesoyuz. Miner. Obsh., 1977, 4, pp. 476-481 (in Russian).
3. Samoilovich L.A. Relationship between pressure, temperature and density of water-salt solutions. M.:VNIISIMS, 1968, p.47 (in Russian).
4. Senderov E.E. and Khitarov N.I. Zeolites, their synthesis and conditions of formation in nature. M.: Nauka, 1970, p. 283 (in Russian).
5. Euellmer F.J. X-ray intensity measurements of perthitic materials. II. Data from natural alkali feldspars. J. Geol., 1960, V.68, N3, pp.307-319.
6. Wright T.L. X-ray and optical study of alkali feldspar. II. An X-ray method for determining the composition and structural state from measurement of 2Θ values for three reflections. Amer. Miner., 1968, v.53, N1/2, pp. 88-104.

[#]Kiseleva I.A., Ogorodova L.P., Mel'chakova L.V. New data on thermodynamic properties of calcium zeolite-stellerite.

key words [*zeolite stellerite thermodynamic calorimetry enthalpy of formation*]

Stellerite $Ca_4(Al_8Si_{28}O_{72})\cdot 28H_2O$ - a calcium zeolite of the heulandite group occurs in hydrothermal veins, geothermal fields, in voids and joints of effusive rocks and is characteristic of the lowest stages of metamorphism. Its thermodynamics is studied insufficiently: only recently its heat capacity at low temperature and entropy have been determined [1]. No data are available on enthalpy and free Gibbs energy of stellerite formation.

The enthalpies of formation and dehydration were obtained using a Tian-Calvet high-temperature heat-flux microcalorimeter. Drop-solution calorimetric method was used to determine the enthalpy of formation of stellerite. This method was chosen to avoid decomposition of zeolite at the calorimeter temperature prior to dissolution. The samples were dropped from room temperature into molten $2PbO\ B_20_3$ at 975 K. Heat of dehydration was obtained using transposed temperature-drop calorimetry. The heat effect contained two contributions: the enthalpy of dehydration at 975 K and the heat content of zeolite. When the solid decomposition products were dropped into the calorimeter, the heat effect contained only the heat content of the dehydrated zeolite.

The studies were performed on a natural sample of stellerite (Savinskoye deposit, East. Siberia) compositionally close to the theoretical one, according to [2]. The results of the calorimetric study of stellerite at 975K are listed in the Table, the errors are expressed in 95% significant interval, the number of the determinations is given in brackets. The thermodynamic properties were calculated

[#] The work was sponsored by the RFBR (Grant N 98-05-64219)

for a simplified stellerite formula, containing 18 oxygen atoms: $Ca_{1.02}Al_{2.01}Si_{6.98}O_{18}\cdot 7.04H_2O$.

Table. Experimental calorimetric data at T=975K.

Compound	Value being measured	kJ/mol
Stellerite	$(H^o_{975}-H^o_{298.15})+\Delta H^o_{deh.,975}$	1109.4±1,6 (6)
Stellerite	$(H^o_{975}-H^o_{298.15})+\Delta H^o_{sol\cdot 975}$	1049.8±7.0(8)
Dehydrated stellerite	$(H^o_{975}-H^o_{298.15})$	409.3±1.6 (5)
Corundum	$(H^o_{975}-H^o_{298.15})+\Delta H^o_{sol.\ 975}$	107.9±1.0(8)
Quartz	$H^o_{975}-H^o_{298.15})+\Delta H^o_{sol\cdot 975}$	39.1±0.3(9)
Calcite	$(H^o_{975}-H^o_{298.15})+\Delta H^o_{sol\cdot.975}$	193.4±0.7(10)

The enthalpy of the stellerite dehydration at T=298.15 K according to the reaction: stellerite = dehydrated stellerite +7.04 H_2O(l) is equal to 214.5±2.2 kJ/mol, which corresponds to the endothermal effect of about 30 kJ/mol as 1 mole of water has escaped from the zeolite framework.

The standard enthalpies of formation from oxides and elements at T=298.15 K for stellerite of the composition $Ca_{1.02}Al_{2.01}Si_{6.98}O_{18}\cdot 7.04H_2O$ (M.m.=705.86 $g\cdot mol^{-1}$) are, respectively, -200.1±7.5 and -10909.1±10.3 kJ/mol. The obtained values of the enthalpies were corrected to the compositions of ideal stoichiometry. The use of the experimental data [1] enable us to calculate all the thermodynamic characteristics of stellerite of the theoretical composition $CaAl_2Si_6O_{18}\cdot 7H_2O$ (M.m.=704.74 $g\cdot mol^{-1}$) to be $S^o_{298.15}$=800.3 J/mol·K, $\Delta H^o_{deh.\ 298.15}$=216.1±2.2 kJ/mol, $\Delta fH^o_{298.15}$=-10887.4+10.4 kJ/mol, $\Delta fG^o_{298.15}$=-10016.1 ±10.4 kJ/mol.

References:

1. Paukov I.E., Belitsky I.A., Fursenko B.A., Koval'skaya Yu.I. (1997) Thermodynamic properties of natural stellerite at low temperatures. // Geochim., N.10, pp.1070-1072.
2. Gottardi G., Galli E. (1985) Natural zeolites. // Berlin: Springer, 409 p.

#Kotel'nikova Z.A. Solutions of alkali and alkaline earth chlorides under high temperatures based on the data on synthetic fluid inclusions.

key words [*synthetic fluid inclusion*]

Fluid inclusions of solutions, containing diverse concentrations of NaCl, KCl, $CaCl_2$, $BaCl_2$, and $SrCl_2$, were synthesized in quartz by the method of crack healing. Study of the inclusions allowed to determine a phase state of the solutions and, in the case of their heterogenization to liquid and vapor, to measure salt concentration in them. Concentration of the liquid phase (phase L) was determined by temperature of crystal dissolution at heating, whereas composition of gas phase (phase V) was identified by cryometry.

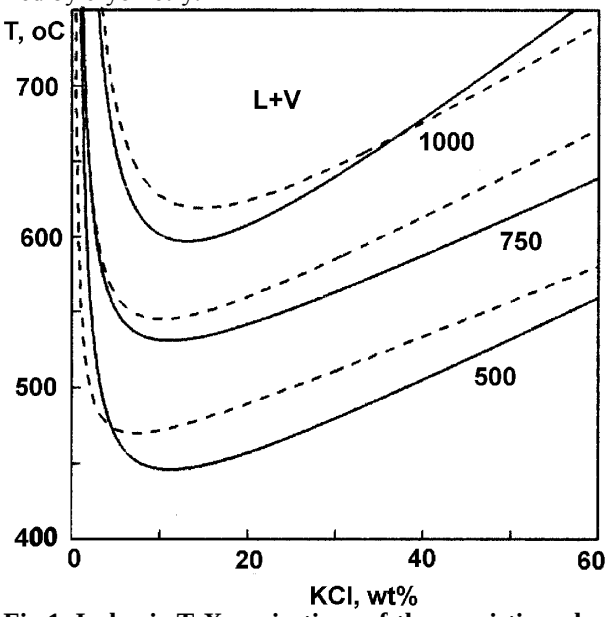

Fig.1. Isobaric T-X projections of the coexisting phases in the system KCl-H_2O (solid) and NaCl-H_2O (dash) [Bodnar et al., 1985] obtained from synthetic fluid inclusions data.

Fig.1 shows position of isobars 500, 750, and 1000 bar in the T-X cross section for the system H_2O-KCl; curves for the system H_2O-NaCl (Bodnar et al., 1985) are shown for comparison. It is seen, that at equal pressure the region of heterogenization to liquid and vapor phases in the KCl-bearing system is displaced to lower temperatures, this displacement being decreased with increasing pressure. At 450-650^{O}C NaCl-bearing solutions are homogeneous in the whole compositional interval at pressures above 450 and 1070 bar, respectively. These pressures increase up to 520 and 1250 bar for KCl-bearing solutions.

P-V-T data for the solutions with 15 wt % of KCl were obtained using the method by Bodnar and Sterner (1985). Inclusions were synthesized, and temperatures of homogenization were measured at pressures 500, 1000, and 2000 bar and temperatures 350-500^{O}C. According to Bodnar and Sterner (1985), correction for quartz thermal expansion influence density value in the third sign after decimal point. We disregard them, for total errors of monitoring of temperature of inclusion synthesis is higher. Slopes of isochors were obtained on the basis of measured temperatures of homogenization of the inclusions, synthesized at different pressures, while density values and vapor pressure on the liquid-vapor curve are taken from

The study was fulfilled under support of Russian Foundation for Basic Research (projects N99-05-65225 and 97-05-65886).

Khaibullin and Borisov (1966). Fig.2 shows the obtained results.

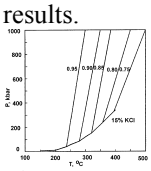

Fig.2. P-T projection showing isochores (g/cm3) of 15 wt% KCl solutions determined from synthetic fluid inclusions. Densities along the liquid-vapor curve are from Khaibullin and Borisov (1966).

Mixing two homogeneous chloride solutions (K-Ba) or homogeneous solution with heterogeneous one (Na-Ba, Ba-Sr) leads to fluid heterogenization. Thus, addition of a third component to a binary system favors fluid heterogenization.

The SFI method allows to estimate the critical parameters of high-temperature solutions (Knight and Bodnar, 1989; Oakes et al., 1994). Inclusions, which captured fluid of critical density, demonstrate homogenization with immediate disappearance of meniscus, solutions of density above critical are homogenized to liquid, below critical - to gas to the left and to the right from the critical isochor, respectively. The critical isochor can be drown through two points of critical homogenization. Its intersection with the boundary of the two-phase region gives value of critical pressure. Such approach was applied in the experiments with decreasing step both by temperature and pressure for measurements of critical parameters of $CaCl_2$-bearing solutions with 26 and 29 wt % of $CaCl_2$. Results of the experiments at 1 and 2 kbar allowed to draw the critical isochor. After that, experiments were performed for the same solution at temperatures 600 and 700^OC at constant temperature, but at varying pressure with a step 150 bar. At densities above the critical at decreasing pressure the homogenization to liquid is followed by two-phase region, which is easy to identify by appearance of solid wollastonite. At densities below the critical homogenization to gas is also followed by two-phase region. Critical pressure occurs between these parameters. The critical parameters for $CaCl_2$ solution, i.e. 610^OC, 1350 bar at 26.0 wt % and 680^OC, 1600 bar at 29.5 wt %, were obtained by this method.

An error of the method is large, not least than 10^O and 100 bar. The major contribution is provided by the inaccuracy in temperature and, especially, pressure control. However, the method allows to estimate the critical parameters, that is valuable in the interpretation of natural inclusions.

Alekseyev V.A., Medvedeva L.S. Secondary mineral precipitation mechanisms in the sanidine-for-albite substitution reaction.

key words [*albite substitution precipitation mechanism*]

We have earlier found that at 300^oC and pH 9 the sanidine-for-albite substitution $NaAlSi_3O_8 + K^+ = KAlSi_3O_8 + Na^+$ (Ab→San) reaction rate (r) decreases as the distance (L) between primary albite and secondary sanidine seed crystals increases [1]:

$$r = kL^{-0.42} \quad (1),$$

where $k=1.4x10^{-10}$, r is given in mol/sec, and L is given in m . The eq (1) was derived for the surface sites of albite (S_{Ab}) and sanidine (S_{San}) equal respectively to 0.278 and 1.112 m^2/kg of the solution ($S_{San}=4\ S_{Ab}$). The dependence manifested itself to 1 mm. At a greater distance the accelerating effect of the seed crystals on the reaction rate ceased. The hypothesis of the microblock growth of sanidine was suggested to explain this dependence. It was believed that the reaction rate controlling stage was diffusion of sanidine nuclei, generated in the solution volume, to the seed crystals. The aim of this work has been to experimentally verify this hypothesis by separating sanidine nuclei, if they from, and establishing the relationship between their mass and size and the reaction rate.

Crushed fractions (0.05-0.1 mm) of albite, sanidine and quarts rinsed to be clean of fine particles, were used in the runs. These minerals together with 0.1 m $KHCO_3$ solution were heated in evacuated platinum capsules at 300^oC and pH 9 for a preset time period. The run conditions (fig.1) where analogous to those of our earlier studies wherein solutions and solid phases had been analyzed [1,2]. In the runs without quartz (filled symbols) the albite-to-sanidine transformation reaction was preceded by a rapid congruent stage of albite dissolution (coincident with the ordinate axis) and a long induction period (horizontal portion of the curve with rhombs) during which the reaction was suspended. In the runs with quartz (open symbols) the high concentration of silica in the solution (0.02 m) favoured the formation of a supersaturated solution with respect to sanidine and its precipitation in the very beginning of the albite dissolution. These differences aside the Ab→San reaction rate in the runs with and without quartz was the same. This fact is indicated by the same slopes of the kinetic curves in two pairs of run series arranged on the left and right sides. So, quartz is actually an inert mineral for the reaction being studied and its use to set the distance between albite and sanidine is quite correct.

In all the runs there formed a fine sanidine precipitation that we separated from a coarser fraction of the initial mineral by lightly shaking the content of the capsules with water and then decanting it onto a nuclear ultrafilter (the pore size is 30 nm). The fine precipitation formed through a homogeneous nucleation in the solution made up only a small fraction of the neogenic (4-20%). Sanidine segregations in the fine precipitation are from 0.05 to 3 μm in size, i.e. they retain capacity for the Brownian diffusion in the solution (fig.2). Despite the increased run duration, in each fine precipitation, along with larger segregations there were always small sanidine segregations that attested that the nucleation process proceeded throughout the observable time period. As the size grew, the segregations shape changed from spheric to elongated tabular and isometric. Their mass increased with increasing reaction rate. The characteristic were aggregates and intergrowths of crystals, in parallel crystallographic orientation included. These facts evidence for the microblock sanidine growth.

The most likely place for sanidine nucleation is the solution located near active sites of albite dissolution, i.e. near surface defects. The calculations show that here the solution supersaturation in sanidine ought to be much higher than far from the active sites.

In the presence of seed crystals the neogenic sanidine precipitates preferentially on them and not on albite. In this case from albite towards seed crystals there have to from a stable flow of sanidine nuclei, and at the albite and sanidine surface there have to form 2 diffusion zones with the nuclei concentration gradients. In each zone the 1-st Fick's law must hold:

$$\mathbf{r_{Ab} = -DS_{Ab} (m-m_{Ab})/l} \quad \textbf{(2)}$$

$$\mathbf{r_{San} = DS_{San} (m-m_{San})/l} \quad \textbf{(3)}$$

where r_{Ab} and r_{San} are diffusion flows in these zones, m_{Ab}, m_{San}, and m are the concentrations of sanidine particles at the surfaces of albite, sanidine and at the external boundary of the zones, l is the thickness of the zones, D is the diffusion coefficient of sanidine particles:

$$\mathbf{D = RT/(3\pi\eta Nd)} \quad \textbf{(4)}$$

Here R is the universal gas constant, T is the absolute temperature, N is the Avogadro number, d is the particle diameter, η is the dynamic solution viscosity. Under the steady-state conditions of the flows $r_{Ab} = r_{San} = r$. From the equality of the expressions (1)-(3) at $m_{San} = 0$ it follows:

$$\mathbf{m = kL^{0.58}/(2DS_{San})} \quad \textbf{(5)}$$

$$\mathbf{m_{Ab} = m(S_{Ab} + S_{San})/ S_{Ab}} \quad \textbf{(6)}$$

Calculations using (5) and (6) performed for the particle size close to the maximal one (d=1μm) yield the m and m_{Ab} values, also close to maximal. Nevertheless, the total mass of sanidine particles calculated from these concentrations and the solution volume in the runs (4 ml) is one order of magnitude smaller than their mass on the filters. So, even a small fraction of fine precipitation, forming in the runs, is capable of ensuring the observable reaction rate via the Brownian diffusion of sanidine particles. With the distance in excess of 1 mm between the diffusion zones there forms a convective zone whose width is of no effect on the reaction rate. With the distance L less than 1 mm the diffusion zones get overlapped. According to the 1-st Fick's law, this ought to lead to an increase of the reaction rate in proportion with L^{-1} and not $L^{-0.42}$ as in the experimental dependence. The both dependencies overlap in the case that m and m_{Ab} decrease with decreasing L according to eqs (5) and (6).

This is a possibility if with the approach of seed crystals to the homogeneous nucleation zone a still greater fraction of sanidine precipitates from the true solution directly on seed crystals. This mechanism has to be dominant on the AB portion (fig.3) that is attested by the independence of r on L. On the BD portion the experimental dependence $r=kL^{-0.42}$ is expanded into 2 dependencies which correspond to 2 competing mechanisms: diffusion of sanidine nuclei in the solution ($r_1 = k_1L^{-1}$) and surface reactions, i.e. precipitation of sanidine from the true solution ($r_2 = k_2$).

Inasmuch as the two mechanisms are competing for one source, namely, supersaturated solution, and act in parallel, the actually observable reaction rate must be the sum of the rates, corresponding to each mechanism, multiplied by their participating fractions, α and (1-α):

$$\mathbf{r = \alpha r_1 + (1-\alpha)\, r_2} \quad \textbf{(7)}$$

After substituting the r, r_1, and r_2 values, we find α:

$$\mathbf{\alpha = (kL^{-0.42} - k_2) / (k_1L^{-1} - k_2)} \quad \textbf{(8)}$$

The calculations from (7) and (8) have shown that as L grows, the participating fraction of the diffusion mechanism α increases from 0.42 to 0.86, but the fraction of sanidine having precipitated by this mechanism per unit time, i.e. $\alpha r_1/r_2$ decreases from 0.42 to 0.06. Some part of sanidine, precipitated from the true solution acts as a cement fastening sanidine nuclei blocks and their aggregates of different size and form among themselves and, also, partly fills in gaps, thus masking the crystal block structure.

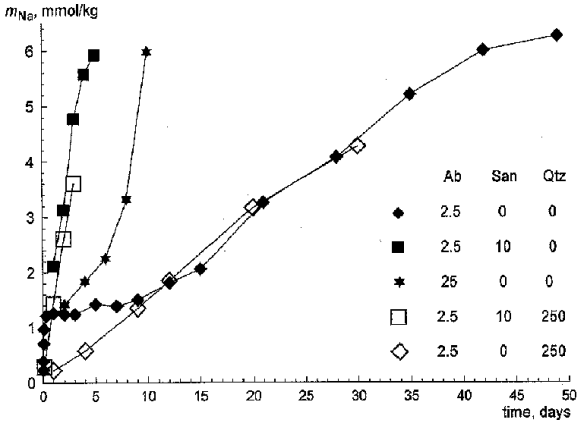

Fig.1. Temporal concentration change a sodium solution resultant from congruent and incongruent (with the formation of sanidine) dissolution of albite at 300°C and pH 9 at different mineral masses ratios (g/kg solution) [1,2]. Ab-albite, San-sanidine, Qtz-quartz. Grain size 0.05-0.1μm.

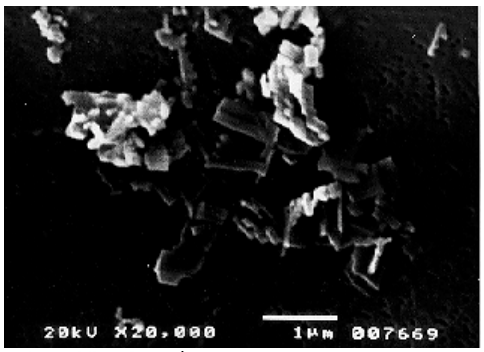

Fig.2. Microphotograph of the surface of neogenic sanidine nuclei generated in the solution volume by the reaction Ab →San. One can see the intergrowth of a nuclei fraction in parallel crystallographic orientation. Scanning electron microscopy. The scale line below corresponds to 1 μm.

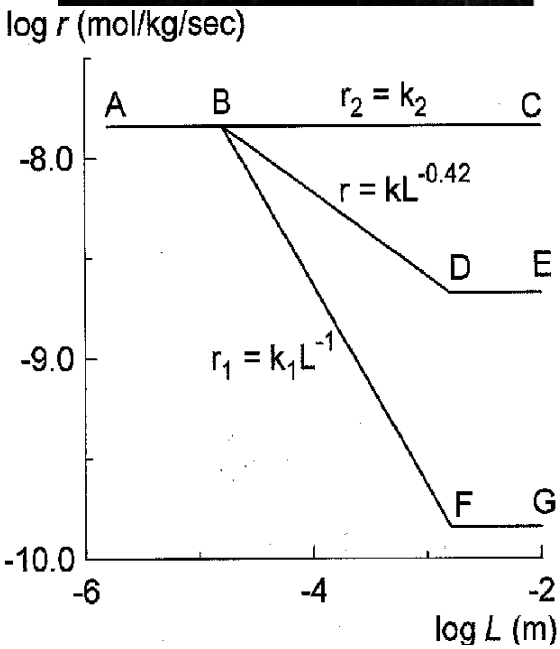

Fig.3. Reaction rate (r) of Ab→San vs the distance (L) between the initial albite and sanidine seed crystals: ABC - at the control of r by surface reactions and sanidine precipitation on the seed crystals from the true solution; ABDE - actually observable dependence [1]; BFG - at the control of r by diffusion of sanidine particles, nucleated in the solution volume at the albite surface, to sanidine seed crystals.

Reference:

1. Alekseyev V.A., Medvedeva L.S. (1999) // Geochemistry International (in press).
2. Alekseyev V.A., Medvedeva L.S. (1996) // Geochemistry International, V.33, N.12, pp.1070-1082.

[#]**Malinin S.D., Baranova N.N., Zotov A.V., Akinfiev N.N.** **Experimental study of scheelite solubility at 400°C and 500 bar. Modeling of the effect of nonpolar gas component on solubility.**

key words [*scheelite solubility thermodynamic properties mixed fluid*]

The available experimental data on solubility of scheelite under hydrothermal conditions are disputable [Foster, 1977]. The aim of this work has been to refine thermodynamic properties of W-bearing particles $WO_4^{2-}, HWO_4^-, WO_3^0$ and to estimate the effect of a nonpolar gas on solubility of scheelite in alkali solutions.

The runs were conducted in 15-20 ml autoclaves (BT-8 alloy) at T=400°C and P=500 bar. Synthetic scheelite crystals, 1-2 mm in size, were charged in a cup fixed at the autoclave cover. Alkali solutions were produced from a saturated NaOH solution by diluting it with freshly boiled distilled water. An argon flow was passed through the autoclaves before charging them. The run duration was 8-11 days, in accord with the results of the scheelite dissolution kinetics study. The concentrations of tungsten and calcium were determined in the solutions after quenching the autoclaves, using ISPMS and flame photometry, respectively. The calculation of the scheelite solubility as a function of pH in pure water and mixed (H_2O-N_2) fluids was performed using a modified version of the program BALANCE intended for equilibrium studies in multisystems [Akinfiev, 1986]. The thermodynamic properties of scheelite were borrowed from [Zhidikov, Khodakovsy, 1984], of portlandite from [Akinfiev, 1998]. The water solution included particles of Ca^{2+}, $CaOH^+$, Na^+, $NaCl^o$, Cl^-, OH^-, H^+, HCl^o, $NaOH^o$, N_2^o, $WO_4^{2-}, HWO_4^-, WO_3^0$. The thermodynamic properties of Ca^{2+}, Na^+, $NaCl^o$, Cl^-, Na_2^o, WO_4^{2-} were borrowed from the SUPCRT92 data base [Johnson et al, 1992] of $CaOH^+$ from [Akinfiev, Zotov, 1999], of HCl^o from [Tagirov et al, 1997], the properties of OH^- were calculated from the data of [Marshall, Frank, 1981]. The thermodynamic parameters of $NaOH^o$ were calculated from the results of the work [Ho, Palmer, 1996] , of HWO_4^- from the data on the constants tungstate-ion hydrolysis [Wesolowski, 1984], and WO_3^o - from the $WO_{3,cr}$ solubility experiment [Wood, Vlassopoulos, 1989] at elevated temperatures. The comparison of calculation and experiment is shown in fig.1. An increase in the solubility of scheelite for pH>8 is governed by the reaction $CaWO_{4,cr} + OH^- \Leftrightarrow CaOH^+ + WO_4^{2-}$ with $CaOH^+$ and WO_4^{2-} being dominant in solution. A drastic increase in the concentration of tungstate -ion at pH>9.6 is dictated by an incongruent character of scheelite dissolution followed by the formation of portlandite $Ca(OH)_{2,cr}$.

The experimentally found dependence of scheelite solubility on pH is similar to the calculated one and shows

[#] The work was sponsored by the RFBR (Project N 97-05-64036 and 98-05-64234)

that portlandite forms already from solutions with pH>8.2.

This circumstance points to the necessity of refining thermodynamic properties of tungstate-ion.

The technique for the equilibrium calculation in a mixed fluid, H_2O-N_2, is based on the introduction of corrections to hydration components of chemical potential of water particles and is detailed in [Akinfiev et al, 1998].. An addition of nitrogen (molar fraction X_{N2} = 0.1) not only decreases the scheelite solubility by more than an order but, also alters the dissolution reaction character (fig.2).

The dominant form of tungsten in the solution is, now, hydrotungstate-ion HWO_4^-, and the dissolution reaction follows the course

$$CaWO_{4,cr} + H_2O \Leftrightarrow CaOH^+ + HWO_4^-$$

A subsequent verification of the calculation of scheelite solubility under hydrothermal conditions for mixed H_2O-N_2 fluid in an alkali region will make it possible to refine the Born parameters of WO_4^{2-} and HWO_4^- ions.

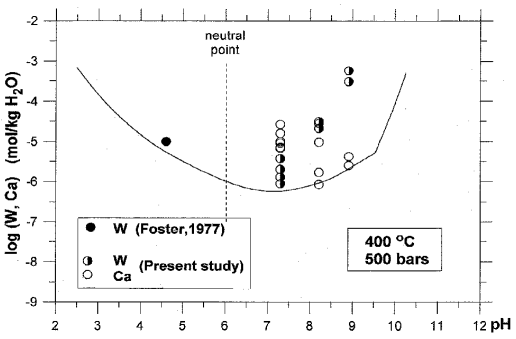

Fig.1. Scheelite solubility vs pH. Symbols are experiment points. Solide line is calcultation

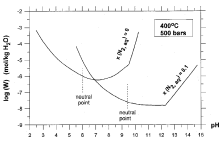

Fig.2. Calculation of scheelite solubility vs pH and N_2 mole fraction

References:

1. Foster P.P. (1977) // Chem. Geol., 20, pp.27-43.
2. Akinfiev N.N., Zotov A.V. (1999) // Geochim Cosmochim. Acta ., in press.
3. Johnson J.W., Oelkers E.H., Helgeson H.C. SUPCRT92 (1992) // Comp. Geosci., 18, pp.899-947.

#Kosyakov V.I., Sinyakova E.F., Shestakov V.A.The investigation of the dependence of sulfur fugacity on the composition in the monosulfide solid solution - pentlandite two-phase field at 600°C.

key words: [*Fe-Ni-S system pentlandite sulfur fugacity*]

The measurements of sulfur fugacity for several monophase and two-phase fields are carried out within the part of isothermal (600°C) phase diagram in the Fe-Ni-S system. The results on the sulfur fugacity dependence on the composition of monosulfide solid solution (mss) and the equilibrium mixture of this phase with pentlandite (pn) at 600°C are given. The samples of 48 and 51 at %S sections are prepared from a mixture of elements in the given proportion, placed into evacuated quartz tubes. After melting, the samples are cooled with the furnace turned off. The fugacity measurements of the samples, further annealed at 600°C, are carried out using a pyrrhotite method. The chemical composition of phases are determined using a Camebax electron microprobe. The phase homogeneity limits and conode positions are determined according to the results of the analysis of equilibrium two-phase samples. The data [1,2], which correlate well with our data, are used during the data processing. The least squares method is used to provide a quantitative description of the results. The limit of mss homogeneity area on the side of sulfur is described by the following equation

$$y = 0.54 - 0.0228\,x + x\cdot(1-x)\cdot(1.088517 + 2.600373\,x)\,0.01, \quad (1)$$

where *y is* S mol.fraction, *x* = Ni mol.fraction/(Ni mol.fraction+ Fe mol. fraction). The limit of mss homogeneity on the side of pentlandite is described by the following equation

$$y = 0.5 + x\,(1-x)\,(0.8261 + 2.4136\,x)\,0.01. \quad (2)$$

The limit of pentlandite homogeneity area on the side of mss is approximated by a linear function

$$y = 0.49002 - 0.0349398\,x. \quad (3)$$

The composition dependence of sulfur fugacity *fs2* for pure pyrrhotine is described by Toulmin's and Barton's [3] equation. On the assumption that the *lgfs2* dependence in mss at y=const, is x-linearly dependent,

$$lgf_{S2} = (1-x)\cdot lg_{S2}^{*} + x\cdot lgf_{S2}^{**}, \quad (4)$$

where lgf_{S2}* and lgf_{S2}** are sulfur fugacities for $Fe_{1-\delta}S$ and $Ni_{1-\delta}S$, where $\delta=(1-2y)/(1-y)$. The dependence of the latter value on the composition is expressed as follows

$$lg_{S2}^{**} = 71.99\,(1 - 0.7443N)^{0.5} - 13.186\,N - 29.786, \quad (5)$$

where N=2(1-y).

The sulfur fugacity dependence on the composition of monosulphide solid solution is shown in Fig. 1. Along the limits of mss homogeneity area, the lgf_{S2} dependence on *x* is more distinct for the samples, enriched in pyrrhotine.

The x-dependence of sulfur fugacity for pentlandite along the limits of its homogeneity area on the side of mss is defined as follows. The positions of five conodes in the area of mss-pn equilibrium and the sulfur fugacity, corresponding to these conodes have been experimentally defined. The obtained dependence of sulfur fugacity on *x* for pentlandite along the limits of the homogeneity area, shown in Fig.2, is approximated by the following equation

$$lgf_{S2} = -52.1399 + 146.998\,x - 120.432\cdot x^2. \quad (6)$$

Using these data, the conode positions in the two-phase mss+pn area are calculated. The values of sulfur fugacity for these conodes are worked out. The calculated conode positions are shown in Fig.1.

This work was supported by the Russian Foundation for Basic Researches (Project N 98-05-65314) and by the program Universities of Russia" (Project "Crystalgenesis" grant N 3H-325-98)

It is expected that the results of the study of the sulfur fugacity dependence on the composition, described in the present report, will be subsequently used to find out the correlation between the forms of occurrence of the platinum elements in sulphide associations. These results are supposed to be used to study the dependence of partition coefficients of these elements on sulfur fugacity and the composition of associations.

References:

1. Naldrett A.J., Craig J.R., Kullerud G. // Econ. Geol., 1967, V. 62, p. 826.
2. Shewman R.W., Clark L.A. // Can. Journal Earth ScL, 1970, V. 7, p. 67.
3. Chemistry of sulphide minerals. Moscow, Mir, 1981, 565p.

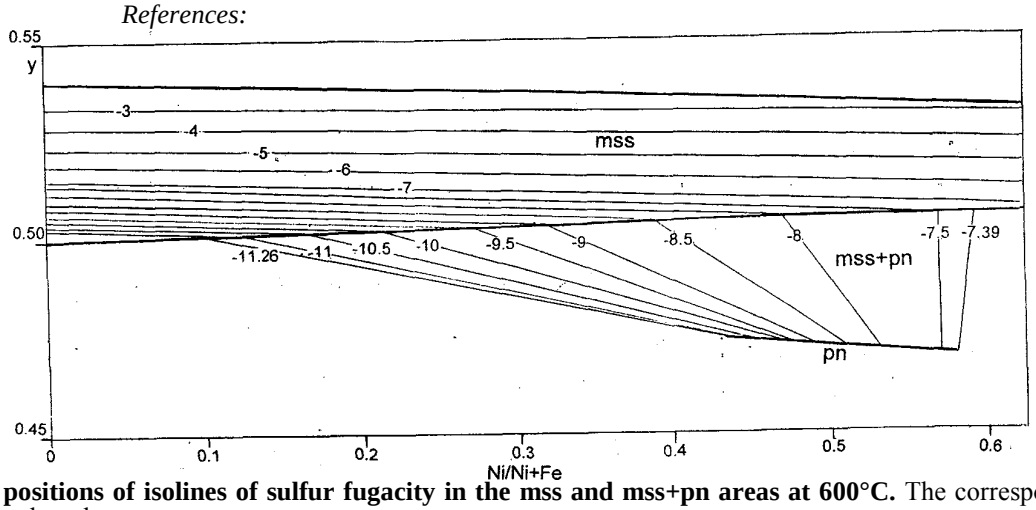

Fig. 1. The positions of isolines of sulfur fugacity in the mss and mss+pn areas at 600°C. The corresponding lgF_{S2} values are numbered.

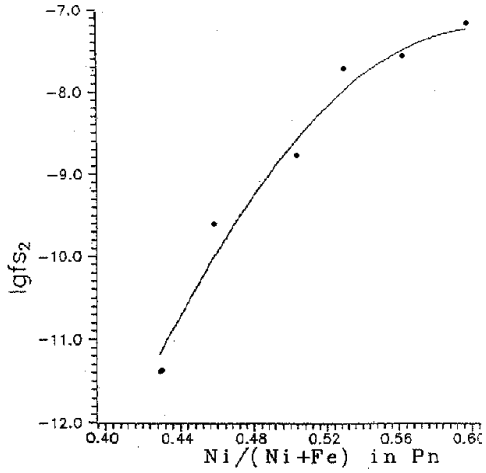

Fig.2. The dependence of sulfur fugacity on the pn-composition at 600°C along the homogeneity boundary

Bychkov A.Yu., Druschitz M.A., Golikova G.V. Experimental study of orpiment solubility in hydrogen sulphide gas.

key words [*solubility gaseous solution hydrogen sulphide orpiment*]

Experimental data have recently been reported on transport of hydrothermal - process components in a gaseous phase. In the work by Migdisov et al., 1998 it was shown that gaseous hydrogen sulphide can actively transport elemental sulphur. To continue those studies we have undertaken to determine the scales and forms of orpiment transport in gaseous hydrogen sulphide.

Lightened titanium autoclaves were used for the runs. Hydrogen sulphide was produced through the interaction of FeS with diluted HCl and purified with NaOH and distilled water, dried by freezing at a temperature -55°C. Hydrogen sulphide was introduced into the autoclave by a freezing procedure at -85°C. Natural orpiment from the Lukhumi deposit, pretreated with NaOH and NaCl, was used. Small crystals were located in glass capsules and fixed in the autoclave with a special holder. In several cases we, analogously, introduced elemental sulphur.

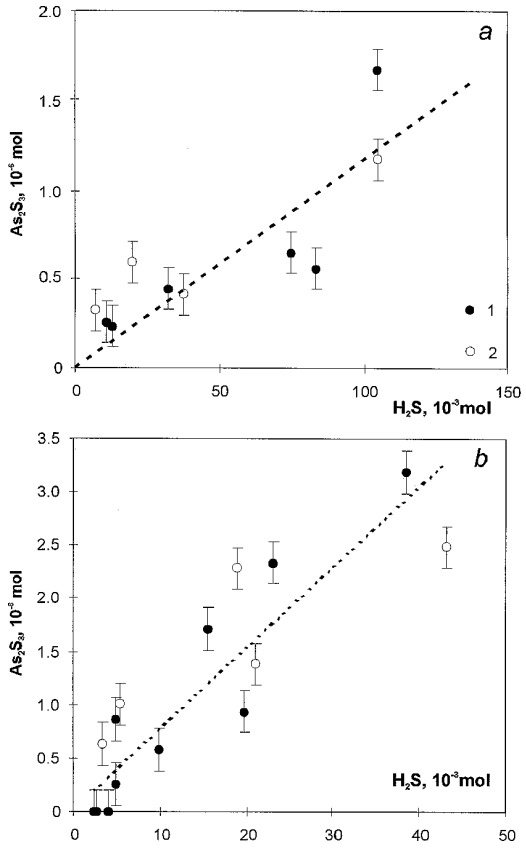

Fig.1. The quntity of transported ipiment with H2S at 160 (a) and 200 (b) °C. 1- system As_2S_3-H_2S; 2-As_2S_3-H_2S-S

The autoclaves were located in a thermostat, the temperature was controlled with a thermometer and thermocouples. The temperature gradient was less than 0.1°C inside. The holding time was 14-20 d. The quenching was performed in air for 10-15 min. As the practice shows, the components are completely rejected from the gas to condense on the walls, but nonisothermal transport is inhibited. After the runs the phases were determined visually in the autoclaves: in the runs without sulphur orpiment crystals were found, in the runs with sulphur-numerous sulphur droplets. In them laminated orpiment was seen under a microscope.

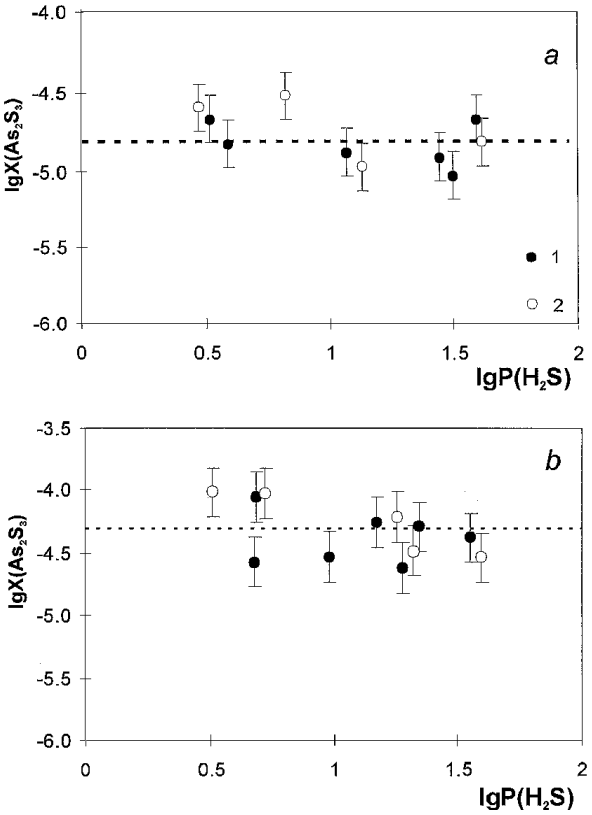

Fig.2. The dependence of logariphms of mole part of As_2S_3 with partial pressure of hydrogen sulphide at 160(a) and 200 (b) °C. 1- system As_2S_3-H_2S; 2-As_2S_3-H_2S-S

The rinsings were performed using a 2M KOH+K_2S solution that dissolves both orpiment and sulphur. The completeness was controlled by repeated rinsings. As a sulphide ion hinders the determination, the samples were preoxidized with a mixture of concentrated sulphuric and nitric acids (1:3). The samples were then evaporated to get rid of HNO_3.

Arsenic in the samples was determined by a photometric and ascorbic acid (Nemodruk, 1976). The measurements were performed on a photoelectrocolorimeter FET-56M provided with a red light filter. The calibration diagram was derived from a series of standard solutions with the concentration from 0.1 to 3 μg/l. The determination uncertainty did not exceed 6%.

The data on vapour pressure in the As_2S_3 system are unreliable and disputable (Hsiao, Schlechten, 1952, Ustyugov et al, 1968). The orpiment evaporation procedure can be represented by the reactions with the formation of AsS polymers:
$2As_2S_3 = As_4S_{4(g)} + S_{2(g)}$ … $2As_2S_{3(s)} = 2As_2S_{2(s)} + S_{2(g)}$ (1)
We, therefore, performed 2 run series, i.e., in the systems As_2S_3-H_2S and As_2S_3-H_2S-S. By adding elemental sulphur, we controlled the degree of the reactions (1) proceeding.

The experimentally obtained values of the orpiment solubility in hydrogen sulphide at temperatures 160°C and 200°C are given in fig.1. In the isotherm the lower limit of the As_2S_3 content at $P(H_2S)=0$ is the calculated concentration

complying with orpiment saturated vapour pressure in the boundary system. These molar quantities of As_2S_3 are below the detection limit of the method employed.

The experimental values are 4-5 orders higher than the calculated ones. An increase in the amount of hydrogen sulphide leads to an increase of the orpiment transport. Hydrogen sulphide is therefore not an inert component but it reacts with orpiment.

This supports the idea of a gas-phase specific reaction occurring between the dissolved material and the solvent solvation of orpiment with hydrogen sulphide. The latter process can be described in the general form by gas-phase stoichiometric reaction:

$$As_2S_3 + mH_2S = As_2S_3 \cdot (H_2S)_m \quad (2)$$

where m is the solvatic number. The thermodynamic constant of this reaction can be conveniently expressed via volatilities of the components:

$$\ln K_f = \ln[f(As_2S_3 \cdot (H_2S)_m)] - \ln[f(As_2S_{3\ P,T}] - m\ln[f(H_2S)] \quad (3)$$

or taking into account:

$$\ln[f(As_2S_3 \cdot (H_2S)_m)] = \ln P_{tot} + \ln[X\ (As_2S_3 \cdot (H_2S)_m)] + \ln[\varphi\ (As_2S_3 \cdot (H_2S)_m)] \quad (4)$$

where φ is the volatilily coefficient of $As_2S_3 \cdot (H_2S)_m$ and introducing the quantity z-the generalized coefficient of the system's nonideality of components and the intermixing nonideality, the equilibrium constant can be written as

$$\ln K_f = \ln[P(As_2S_3 \cdot (H_2S)_m)] - \ln[P(As_2S_3)_{P,T}] - m\ln[f(H_2S)] - \ln Z$$

$$\ln K_f = \ln P_{tot} + \ln[X(As_2S_3 \cdot (H_2S)_m)] - \ln[P(As_2S_3)_{P,T}] - m\ln[P(H_2S)] - \ln Z \quad (5)$$

Inasmuch as $(d\ln K_f/d\ln P)_T=0$, then for the S-G equilibrium region, characterized by the constancy of the condensed phase composition, by differentiating the expression in P one can determine the relationship.

Fig.1. suggests that the results obtained for the system As_2S_3 -S-H_2S and those for the system As_2S_3-H_2S are not at significant variance between themselves within experimental uncertainty. One can, therefore, state that the dominant form in the gas phase will be an $As_2S_{3\ m}(H_2S)$ particle. In order to determine the solvate number we processed the experimental data in the coordinates lgP(H_2S) - lgX (As_2S_3), fig.2. The mole fraction of orpiment in the gas is independent of partial pressure of hydrogen sulphide, which corresponds to m-1=0 or m=1. An $As_2S_3 \cdot H_2S$ particle will be dominant in the gas phase. The calculated complexing reaction constant will be: $As_2S_{3\ (s)} + H_2S_{\ (g)} = As_2S_3 \cdot H_2S_{\ (g)}$ at 160°C lgK=-4.8±0.3 at 200°C lgK=-4.3±0.2.

Conclusions

1. The processes of solvation of orpiment with hydrogen sulphide have been shown to proceed very extensively.

2. The molar fractions of As_2S_3 in the gas in the system with elemental sulphur and without it do not differ and are independent of the partial pressure of H_2S. This suggests that the gas complex $As_2S_3 \cdot H_2S$ is stoichiometric.

3. The constant of the reaction $As_2S_{3\ (s)} + H_2S_{\ (g)} = As_2S_3 \cdot H_2S_{\ (g)}$ has been determined to be at 160°C lgK=-4.8±0.3, at 200°C lgK=-4.3±0.2

References:

1. Hsiao C. M, Schlechten A.W. (1952) Volatility and stability of metallic sulphides. // Journal of metals, V. 4, p.65-69.
2. Migdisov Art.A., Sulejmenov O.M., Alekhin Yu.V. (1998) Experimental study of polysulfane stability in gaseous hydrogen sulfide. // Geocemica et Coscmocemica Acta, V.62, p.2627-2635
3. Nemodruk A.A. (1976) Anal. chemistry of arsenic. // M., Nauka press, 260p.
4. Ustyugov G.P., Kudryavtsev A.A., Kuadzhe B.M. (1968) Pressure of saturated arsenic sulfide vapours. // Inorganic Mater., V.4, pp.1338-1339.

[#] Shironosova G.P., Kolonin G.R., Sushchevskaya T.M. Modeling of influence of dilution of tungsten-bearing fluid on its productivity.

key words [*modeling ore -forming fluid tungsten wolframite*]

An analysis of the physicochemical data on high temperature hydrothermal systems, associated with granites, shows that W- and W-Sn-ore formation occurs at a background of their salinity decrease and substitution of chlorine-bicarbonate sodium - potassium-calcium solutions for chloride-sodium ones [1].

The results of isotope composition determination of hydrogen, oxygen of fluids [2,3], elemental and isotope composition of noble gases [4] indicate the entrance into hydrothermal systems of exchange waters having had, originally, a meteoric nature.

Based on these ideas and using a thermodynamic modeling method, we have studied the influence of dilution of an ore-forming fluid on precipitation of tungsten from it in hydrothermal systems at intermixing of solutions of different origin. To this end, in three calculation series, using GBFLOW program, we performed a decrease in the concentration of chlorides and/or fluorides of the initial fluid. The model fluid incorporated NaCl, KCl, HF, H_2S, it was saturated in model granite, $FeWO_4$+$MnWO_4$ mixture and a buffer pair (FeS +FeS_2).

In the first series we imitated a four-stage tree-order dilution of the initial concentration of HF, the concentration of the remaining components being constant, which provided a congruent presence of the basic typical mineral phases (muscovite, fluorite, F-topaz, annite as model proxy of Fe-biotite, scheelite, wolframite of a particular composition, iron sulfides) with an abundance of K-feldspar and quartz. In the

[#] The work has been sponsored by the RFBR (Project N 97-05-65318)

second series we modelled a four-stage 8-fold for NaCl and 10-fold for KCl dilution of chlorides, the concentrations of HF and H_2S being maintained at an optimal level. The comparison of the results shows that the highest (by a factor of 2) initial content of W in the first calculation series decreases dramatically already after the second dilution stage, i.e. by a factor of 13.5, and after the last stage by 69 times. In the second series the concentration of W-decreases but not that strong. In modeling of the fluid dilution in all the initial components (the third calculation series) we have also had a significant decrease of W concentration in the solution, correlating with a change in the F concentration. This is natural and is the reflection of prevalence of a HWO_3F complex among the dissolved forms of W. As a result, the high HF concentrations that persist at first dilution stages ensure also rather high concentrations of W reaching tenth fractions of g/l. By final dilution stages there forms a fluid composition with practically invariable concentrations of the largest number of the components involving not only W and F, but also the background Si, Al, S. In considering the influence of fluid dilution on the composition of equilibrium mineral associations, one can see that relative amounts of Fe and Mn tungstates, fluorite, and F-topaz decrease. The amount of scheelite alone grows. This occurs as a consequence of a decrease of an equilibrium HF concentration because upon dilution fluorite is the first to disappear and then F-topaz do, and the liberated Ca is bound in the form of scheelite (fig.2).

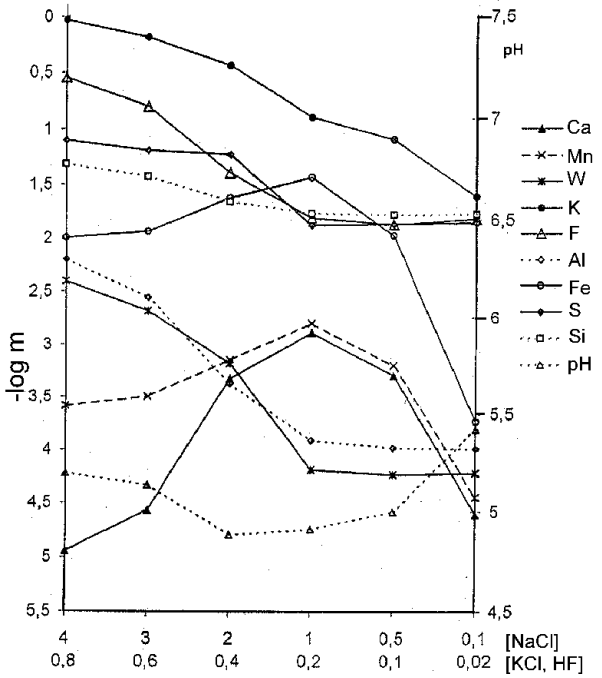

Fig.1. Change in fluid composition in equilibrium with model granite and ore minerals during dilution.

So, where the initial concentrations of chlorides range broadly in the presence of fluorite and other possible F-bearing minerals in the system there is possible the formation of a fluid with a quite high concentration of W (of the order of 70 mg/kg H_2O) decreasing only upon fluorine transferring away from the fluid. Inasmuch as the major from of W transport under these conditions is the HWO_3F complex, the main cause of W precipitation is a decrease of F concentration in a solution due to both the formation of fluorite and dilution of a tungsten-bearing fluid.

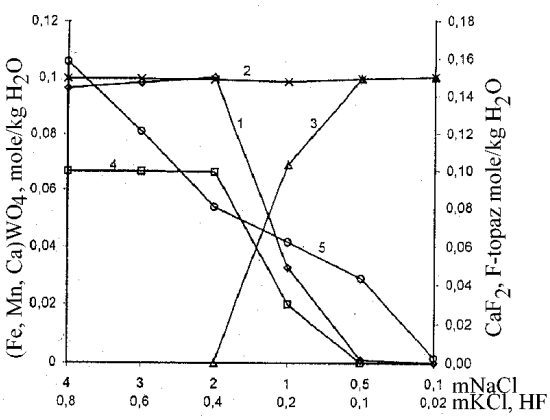

Fig.2. Change in quantities of solid phases during dilution: of wolframites Fe-1, Mn-2, Ca-3, fluorite - 4, F-topaz-5.

References:

1. Sushchevskaya T.M., Spasennykh M.Yu., Matveyeva S.S. et al (1998) Large Sn, Sn-W W deposits (Solnechnoye, Iultin): origin of ore-forming fluids from isotopic and fluid inclusion data. // in Large and unique deposits of rare and noble metals, St-Peters., pp.288-292.
2. Landis G.P., Rye R.O. (1974) Geological, fluid inclusions and stable isotopic studies of the Pasto-Bueno tungsten-base metal
3. Sushchevskaya T.M., Spasennykh M.Yu. (1995) The Iultin tin-tungsten deposit: nature of ore-forming fluids based on oxygen isotope data. // Mineral Deposits, Pasava @ Zak, Balkema, Rotterdam: pp.543-545.
4. Matveyeva S.S., Verkhovsky et al (1991) Nature and evolution of ore-forming fluids of the Akchatau deposit from noble gases and oxygen isotope data. // Geokhimiya, V.3, pp.333-343.

#Kurovskaya N.A., Malinin S.D. Effect of pressure (density) on fluorite solubility in homogeneous NaCl-H_2O fluids

key words [*experiment solubility fluid-crystal equilibria*]

In our earlier works [1-3] we studied the solubility of minerals, i.e. fluorite and scheelite, in the NaCl-H_2O system as a function of pressure at temperatures 600 and 800°C in the regions of both homogeneous and heterogeneous system's state. The major aim of those studies was to established and refine the effect of solubility jump at the moment of fluid decomposition and, also, to establish the regularities of mineral solubility in the heterogeneous region of the system's state.

No estimation was done of the effect of the pressure (density) factor on the solubility of minerals and on the state

The work has been sponsored by the RFBR (Project N 97-05-64036)

of dissolved material in the homogeneous NaCl-H_2O fluid in a broad range of NaCl concentrations.

Table. Experimental data on fluorite solubility in HCl waster solutions

Run N	Concentr. NaCI, mole/kg H_2O	Solution mass, g	Water mass, g	Crystal weight loss mg,	Solubility of CaF_2 n 10^3mole/kg H_2O
600°C 1.0 kbar					
1	1.0	0.40845	0.38590	0.057	1.89
2	2.0	0.77085	0.69022	0.165	0.06*
3	2.0	1.07080	0.95879	0.360	4.81*
4	2.0	0.43100	0.38592	0.120	3.98
5	5.0	0.47865	0.37043	0.330	11.4
6	10.0	-	0.40860	0.750	23.5
7	34.7	-	0.31050	2.017	83.2
800°C 1.6 kbar					
8	1.0	0.37320	0.35260	0.174	6.32
9	5.0	0.46900	0.36296	1.4.38	50.7**
10	5.0	0.47680	0.36899	1.496	51.9**

* - data [1] , ** - data [3]

To solve this problem we have carried out systematic experimental studies of fluorite solubility in homogeneous water solutions of NaCl in a broad concentration range form 1 to 34.7 mol/kg H_2O at 600°C, pressure 1 kbar and in NaCl solutions (1 and 5 mol/kg H_2O) at 800°C, pressure 1.6 kbar. They complement our earlier studies at 600-800°, pressure 2 and 1.6 kbar [3-5]. The results are presented in the table and the figure. Regrettably, the pressure studies were conducted in a narrow pressure range (1-2 kbar at 600°C and 1.6-2 kbar at 800°C). This is because the upper limit of pressures is restricted by the potentialities of the experimental set-up, the lower one is dictated by the boundary parameters between the homogeneous and heterogeneous regions on the phase diagram of the system NaCl-H_2O.

The runs were conducted in a two-chamber high-pressure apparatus with an external heating and isobaric quenching system, using platinum capsules. Synthetic fluorite single crystals were used as samples. The solubility was defined by the single crystal weight loss technique. For the detailed description of the technique see in [4].

The linear dependence of fluorite solubility on the concentration of NaCl has been established in logarithmic scale throughout the investigated range of concentrations at 600°C and pressure 1 kbar (fig). The constancy of the isotherm-isobar slope is detectable at pressures 1 and 3 kbar (600°C) and 1.6 and 2 kbar (800°C). This attests to the invariability of the composition of the dissolved mineral substance particles which in earlier studies in the system CaF_2(k)-NaCl-H_2O [4,5] at 600-800°C, P=2 kbar were identified as neutral complexes of binary mixed salt types ($NaFNaCl^o$).

It has been found that the solvent action of the fluid increases however insignificantly with growing pressure. So, a pressure growth from 1 to 2 kbar at 600°C leads to a solubility increase by approximately 0.2 log un, at 800°C it is still smaller (within an experimental error). The observable relatively small effect of pressure on the solubility of fluorite in the homogeneous NaCl-H_2O fluid indirectly supports the earlier suggestion about the generation upon fluorite dissolution of neutral particles of complex mixed composition.

It has been thus established that the density (pressure) in the studied range (1-2 kbar) does not affect appreciably the state of dissolved substance in the homogeneous fluid and the solvent action of fluid.

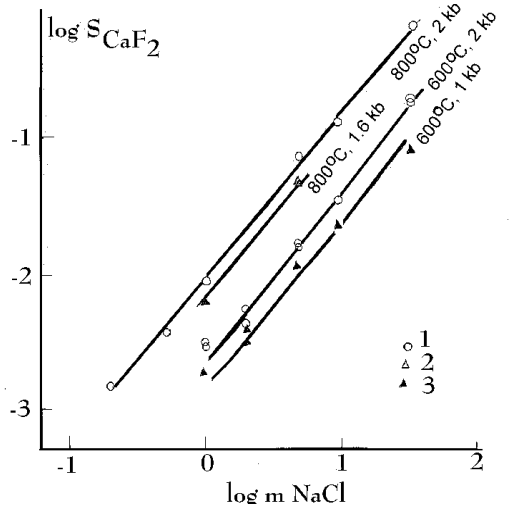

References:

1. Malinin S.D., Kurovskaya N.A. (1996)// Geokhim., N1, pp.1-8.
2. Malinin S.D., Kurovskaya N.A. (1998)// Geokhim., N3, pp.324-328.
3. Malinin S.D., Kurovskaya N.A. (1999)// Geokhim., N1, pp.1-9.
4. Malinin S.D., Kurovskaya N.A. (1992)// Geokhim., N1, pp.1473-1482.

5. Malinin S.D., Kurovskaya N.A. (1996)// Geokhim., N1, pp.1183-1187.